*Desalination and Water Treatment*
www.deswater.com
doi: 10.1080/19443994.2013.866054

53 (2015) 2059–2069
February

Taylor & Francis
Taylor & Francis Group

# Preparation of porous membrane by combined use of thermally and chemical reaction-introduced nonsolvent-induced phase separations

Wentao Yang, Zhan Wang*, Yuenan Zhou, Lina Cheng, Qian Zhang, Ximing Zhang

*College of Environment and Energy Engineering, Beijing University of Technology, Beijing 100124, China*
*Fax: +86 10 67391983; email: wangzh@bjut.edu.cn*

Received 19 May 2013; Accepted 27 October 2013

ABSTRACT

Microporous polyacrylonitrile membranes were prepared via the combination of thermally and chemical reaction-introduced nonsolvent-induced phase separations (TIPS and CRINIPS). In the membrane preparation, glacial acetic acid (GA) and aqueous solution of 2 wt.% sodium bicarbonate were used as additive and coagulation media, respectively, and chemical reaction between GA and sodium bicarbonate resulted in uniform microporous membranes. Pore connectivity and asymmetry were significantly improved when coagulation bath temperature was lowered to 15°C. The fouling mechanisms of the prepared membrane were analyzed by nonlinear regression method and cake filtration model was the most appropriate for the membrane prepared via combining TIPS and CRINIPS. The pore structure was made connective and asymmetric by using a 15°C aqueous solution of 2 wt.% sodium bicarbonate as coagulation media in membrane precipitation process, and the average pore size reduced from about 0.125 to 0.097 μm while decreasing the glass plate temperature from 80 to 20°C.

*Keywords:* Thermally induced phase separation (TIPS); Chemical reaction-introduced nonsolvent-induced phase separation (CRINIPS); PAN; Porous membrane

## 1. Introduction

To date, membrane technologies were extensively applied in every industrial sector including energy, environmental, electronic, chemical, and biotechnology areas due to their remarkable advantages, such as their excellent stability, high efficiency, low energy requirement, and ease of operation [1], Much effort is being devoted to investigate new membrane preparation methods to enhance the performance of membranes, such as anti-fouling properties, high mechanical strength, and good chemical resistance.

Several methods are employed in the preparation of porous membranes including phase separation [2–6], sintering [7,8], track etching [9,10], and other methods [11–14]. Nowadays, most of the commercial membranes are manufactured via phase separation methods because of their simplicity, flexible production scales and the low cost of production [15]. Phase separation can be defined as a demixing process where the initially homogeneous polymer solution is transformed in a controlled manner from a liquid to a

*Corresponding author.

solid or liquid state [16,17]. The transformation can be induced by the removal of thermal energy or existence of nonsolvent. The former is named thermally induced phase separation (TIPS), while the latter is nonsolvent-induced phase separation (NIPS).

In recent years, TIPS has aroused widespread attention due to its intrinsic advantages over NIPS process. The TIPS process is driven by heat transfer rather than mass exchange. Many polymers have been applied for the fabrication of membranes through TIPS process, such as polyacrylonitrile (PAN) [18] cellulose acetate (CA) [19], polypropylene (PP) [20,21], polyethylene (PE) [22], and poly (ethylene-co-vinyl alcohol) (EVOH) [23]. Apart from TIPS, nonsolvent-induced phase separation NIPS is another useful technique for the preparation of polymeric membranes from phase separation process. It has been widely applied in the preparation of microfiltration, ultrafiltration, nanofiltration, and reverse osmosis membranes. The NIPS process can be classified into air-casting of a polymer solution, precipitation from the vapor phase, and immersion precipitation (IP) [24]. The most commonly employed method to fabricate membranes is IP process where a polymer solution is cast on a suitable substrate, then immersed in a coagulation bath containing a nonsolvent.

Recently, many researchers enhanced the performance of the membrane prepared by the means of introducing chemical reaction in IP process, i.e. CRINIPS. Wang et al. [25] used the chemical reaction between the additive ($CH_3COOH$) of casting solution and aqueous solution of $Na_2CO_3$ in the coagulant to produce $CO_2$, which was confirmed to play an important role in the membrane morphology and performance. Wang et al. [26], Liang et al. [27], and Zhou et al. [28] also applied CRINIPS to control the pore size of porous membranes. They pointed out that carbon dioxide gas produced by a reaction between glacial acetic acid in the casting solution and salt in coagulation medium can improve the pore size distribution of the membrane. Besides, researchers prepared porous membranes via combination of thermally and nonsolvent-induced phase separations (TIPS and NIPS). Matsuyama et al. [29] first used this method to prepare PMMA porous membrane. They found that the membrane obtained after the short immersion period had larger pores near the top surface due to NIPS and smaller pores near the bottom surface due to TIPS. Yen et al. [30] prepared poly (caprolactone) (PCL) nanoporous membranes via the combination of TIPS and NIPS to achieve the zero-order release rate and Tanaka et al. [31] also used this method to prepare asymmetric porous poly(l-lactic acid) membranes.

Up till now, many research have concentrated on the preparation of membranes via IP and TIPS, respectively. To the best of the authors' knowledge, few studies have paid attention to the preparation of porous membranes via the combination of chemical reaction-introduced nonsolvent-induced phase separation (CRINIPS) and TIPS. Therefore, in this study, porous PAN membranes were produced via the combination of TIPS and CRINIPS. The fouling models for membranes prepared by different membrane formation mechanism were analyzed. The effects of coagulation bath temperature and substrate temperature on the pure water flux, pore size distribution, and BSA retention were investigated.

## 2. Experimental

### 2.1. Materials

In this study, PAN as membrane material was purchased from Ande Membrane Separation Technology & Engineering (Beijing) Co., Ltd. The solvents — DMF, acid ($CH_3COOH$), and $NaHCO_3$ were purchased from Tianjin Fuchen Chemical Reagent Factory. N-butanol as santomerse was purchased from Beijing Chemical Engineering Factory. Bovine serum albumin (BSA), used for determining the retention of prepared membrane, was purchased from Beijing Microorganism Culture Medium Manufacturing Corporation, and its isoelectric point of pH is 4.8.

### 2.2. Preparation of membranes by phase separation

PAN membranes were prepared using the combination of thermally and chemical reaction-introduced nonsolvent-induced phase separations. The preparation process for casting solution was as follows: first, glacial acetic acid (GA) was dissolved in DMSO in mass ratio of 8:1 under certain stirring speed until completely dissolved; second, PAN at suitable concentration (e.g. 18 wt.%) was dissolved in this mixed solution under certain stirring speed until thoroughly dissolved to ensure that it was clear and homogeneous; and at last, the casting solution was placed in the vacuum oven at 50℃ for two days. Then, the casting solution (casting solution temperature was 50℃) was cast on a clean glass plate (30 mm × 20 mm) using a knife under environmental temperature of 50℃ and relative humidity of 30%. Then, the glass plate was immediately immersed in the coagulation bath, which was aqueous solution of 2 wt.% sodium bicarbonate. Meanwhile, the following chemical reaction occurred: $CH_3COOH + NaHCO_3 \rightarrow CH_3COONa + CO_2 \uparrow + H_2O$. After 2 h, the newly

formed membrane on the glass plate was removed from the coagulation bath. In the end, membranes were immersed in deionized water at 25℃ for at least one day to remove the remaining solvent. In this study, porous PAN membranes were prepared in three different ways (Table 1).

### 2.3. Apparatus and tests

#### 2.3.1. Pure water flux and retention of BSA measurements

Pure water flux and BSA retention (0.1 g $L^{-1}$, $R_{BSA}$) analysis were performed in a dead-end cell with membranes effective area of 24.19 $cm^2$ under 25℃ and 0.1 MPa. The setup is shown in Fig. 1.

For the calculation of pure water flux, we can see Eq. (1).

$$J = \frac{V}{S \cdot t} \tag{1}$$

where $J$ is the pure water flux (ml $cm^{-2}$ $h^{-1}$), $V$ is the permeate volume of water (ml), $S$ is the effective area of membrane ($cm^2$), and $t$ is the time of obtaining the required volume (s).

For the calculation of retention of BSA, we can see Eq. (2).

$$R = \left(1 - \frac{C_P}{C_F}\right) \times 100\% \tag{2}$$

where $R$ is the BSA retention, $C_P$ (g/l) and $C_F$ (g/l) are the concentrations of the filtrate and the feed solution, respectively. The $C_P$ (g/l) and $C_F$ (g/l) were measured by a UV spectrophotometer (2800 UV/Vis spectrophotometer).

Table 1
PAN membranes prepared with different parameters

| Sample | PAN wt.% | Casting solution temperature (℃) | Glass plate temperature (℃) | Coagulation bath or chamber temperature (℃) |
|---|---|---|---|---|
| PAN1 | 18 | 50 | 20 | 5[a] |
| PAN2 | 18 | 50 | 20 | 15[a] |
| PAN3 | 18 | 50 | 20 | 25[a] |
| PAN4 | 18 | 50 | 20 | 35[a] |
| PAN5 | 18 | 50 | 50 | 15[a] |
| PAN6 | 18 | 50 | 80 | 15[a] |
| PAN7 | 18 | 50 | 20 | 15[b] |

Notes: [a]Coagulation temperature.
[b]Chamber temperature.

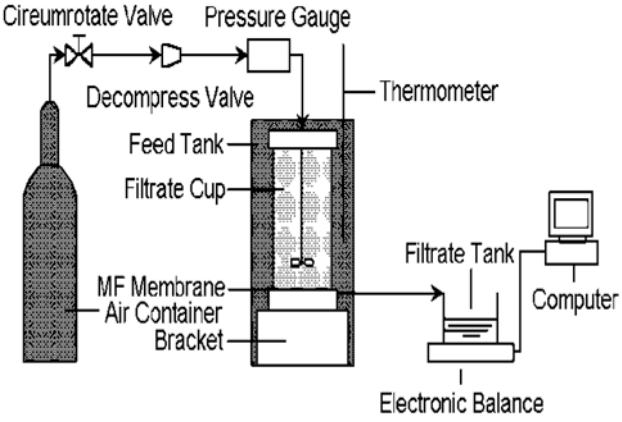


Fig. 1. Schematic representation of the experimental setup.

#### 2.3.2. Pore size distribution and porosity measurements

In this study, pore size distribution analysis was carried out by liquid–liquid displacement technique using n-butyl alcohol-water as solvent pair [32]. For the pore size distribution function, we can see Eqs. (3) and (4).

$$r = \frac{2\sigma \cos\theta}{P} \tag{3}$$

$$f(r) = \frac{P_i(P_{i-1}J_i - P_iJ_{i-1})}{(r_{i-1} - r_i)P_{i-1}\sum_{i-1}^{m}\frac{P_i}{P_{i-1}}(P_{i-1}J_i - P_iJ_{i-1})} \tag{4}$$

where $r$ is the pore radius, $\sigma$ is the surface tension of the n-butyl alcohol-water, $\theta$ is the polymer-n-butyl alcohol contact angle, and $J_i$ is the flux measured at the $i^{th}$ increment where the applied pressure is $P_i$.

For the porosity measurements of PAN membrane carried out by dry/wet method, we can see Eq. (5) [1]:

$$P_o = \frac{W_2 - W_1}{V \cdot d_{water}} \tag{5}$$

where $P_o$ is the porosity of the membrane (%), $W_2$ is the weight of the wet membrane (g), $W_1$ is the weight of the dry membrane (g), $V$ is the volume of the membrane ($cm^3$), and $d_{water}$ is the water density at room temperature (g $cm^{-3}$).

### 2.4. Scanning electron microscopy(SEM)

The membranes prepared were fractured in liquid nitrogen and mounted on a sample holder; then, the sample was coated with Pt/Pd. All the SEM images were obtained on an FEI Quanta (Holland) scanning electron microscopy (SEM).

### 2.5. Determination of the cloud point

The cloud point was measured by visual observation of appearance of turbidity. The PAN-casting solution at 50˚C mixed in a glass vial for 2 h. Then, the vial was quenched in 5˚C water to estimate a possible range of the cloud point. Within the possible range of the cloud point, a vial was placed in an oven at a specific temperature for 1 h to observe the appearance of turbidity in order to determine the exact cloud point [33].

### 2.6. Nonlinear regression analysis

All the parameters in the membrane fouling models were evaluated by nonlinear regression using 1stopt software (China); the objective functions include nonlinear regression coefficient ($R^2$), the sum of squared error (SSE), chi-square ($\chi^2$), and mean square error (RMSE). The smaller values of SSE [34], chi-square, and RMSE indicate better curve-fitting.

## 3. Results and discussion

### 3.1. Coagulation bath temperature effect

In order to investigate the impact of different coagulation bath temperatures (5, 15, 25, and 35˚C) on the performance of membranes prepared with GA, membranes were prepared with 18 wt.% PAN in the casting solution under identical conditions (casting solution temperature of 50˚C, glass plate temperature of 20˚C, gelation temperature of 25˚C, gelation humidity of 30%, and coagulation media of 2 wt.% aqueous solution of $NaHCO_3$). The effects of different coagulation bath temperatures on pure water flux and BSA retention are shown in Fig. 2. The results indicate that the pure water flux increased with the increase in bath temperature, and BSA retention decreased with increase of bath temperature. In addition, Fig. 3 displays the corresponding pore size distribution for the top surface of each of these membranes prepared with the various coagulation bath temperatures. As shown in Fig. 3, the pore size distribution was concentrated in the range of 0.08–0.11 μm for bath temperature of 5˚C, and its peak value is the biggest. As bath temperatures increased to 15, 25, and 35˚C, the ranges of pore size distribution were 0.095–0.10 μm, 0.085–0.15, and 0.1–0.15 μm, respectively. The sequence of the average pore size is 35 > 25 > 15 > 5˚C. In addition, Table 2 lists the porosities of PAN porous membranes prepared with different coagulation bath temperatures. It can be seen from Table 2 that the porosity increased with increasing of bath temperature. Based on Fig. 3 and Table 2, it can explained why pure water flux increased and BSA retention decreased with increasing of bath temperature.

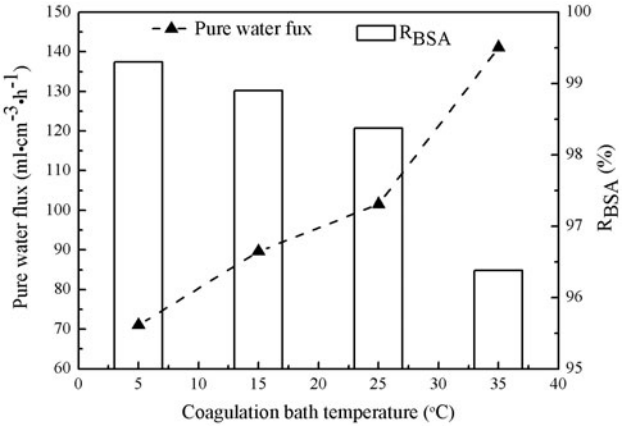


Fig. 2. The pure water flux and BSA retention of the PAN membranes prepared with different coagulation bath temperatures (5, 15, 25, and 35˚C). The casting solution temperature was 5˚C, glass plate temperature was 2˚C, the transmembrane pressure was 0.1 MPa and pure water temperature was 20˚C.

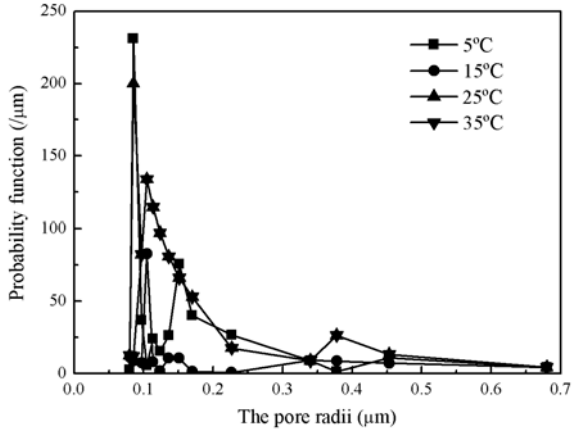


Fig. 3. The pore size distribution of the membranes which were prepared with different coagulation bath temperatures: (a) 5˚C, (b) 15˚C, (c) 25˚C, and (d) 35˚C. Casting solution temperature was 50˚C and glass plate temperature was 20˚C.

Besides, phase inversion contributes to a major characteristic of the membrane, which is asymmetric pore structure [35]. For the asymmetric membranes prepared in this study, both surface layer and sub-layer could affect the pure water flux and BSA retention. Fig. 4 displays the different effects of coagulation bath temperature on cross-section membrane micrographs. These figures show that the colder the coagulation bath temperature, the lesser the pore

Table 2
Porosities of the PAN porous membranes prepared with different water bath temperatures. The casting solution temperature was 50℃ and glass plate temperature was 20℃

| Sample | Coagulation bath temperature (℃) | Porosity (%) |
|---|---|---|
| PAN1 | 5 | 62.3 |
| PAN2 | 15 | 67.8 |
| PAN3 | 25 | 68.3 |
| PAN4 | 35 | 70.5 |

number. As shown in Fig. 4, the pore was not a asymmetric, anisotropic, and interpenetrating network structure when coagulation bath temperature decreased to 5℃ and increased to 35℃, respectively. These may be the consequence of solid–liquid and liquid–liquid demixing when the glass plate was immersed in the cold and hot coagulation bath [36]. Another reason for the different pore morphology under the top surface of membranes may be the different pore formation mechanism which was induced by various coagulation bath temperatures, and these will be discussed in detail in the next section.

### 3.2. Membrane formation mechanism

In order to study the effects of thermally and chemical reaction-introduced nonsolvent-induced phase separations (TIPS and CRINIPS) on membrane performances and its structures, three kinds of membrane formation methods were utilized. The casting solution of 18 wt.% PAN containing GA was chosen and its temperature was maintained at 50℃. As the cloud point of this casting solution was about 20℃, there was only TIPS when the cast membrane was placed in closed chamber. Besides, the CRINIPS occurred when the cast membrane was immersed in 35℃ coagulation bath (2% wt. $NaHCO_3$ (aq.). When the cast membrane was immersed in 15℃ coagulation bath (2% wt. $NaHCO_3$ (aq.), the phase separation occurred involving TIPS and chemical reaction-introduced NIPS (TIPS and CRINIPS).

Fig. 5 shows the effect of membrane formation mechanism on pure water flux, BSA retention and porosity. As shown in Fig. 5, the membrane prepared via TIPS had the lowest pure water flux, porosity and BSA retention, even though its pore size distribution was more uniform than others (Fig. 7). This may be related to the membrane morphology which is illustrated in Fig. 6. It can be seen from Fig. 6 that in both dense surface and cross-section no pore was visible. Besides, as shown in Fig. 5, the pure water flux and

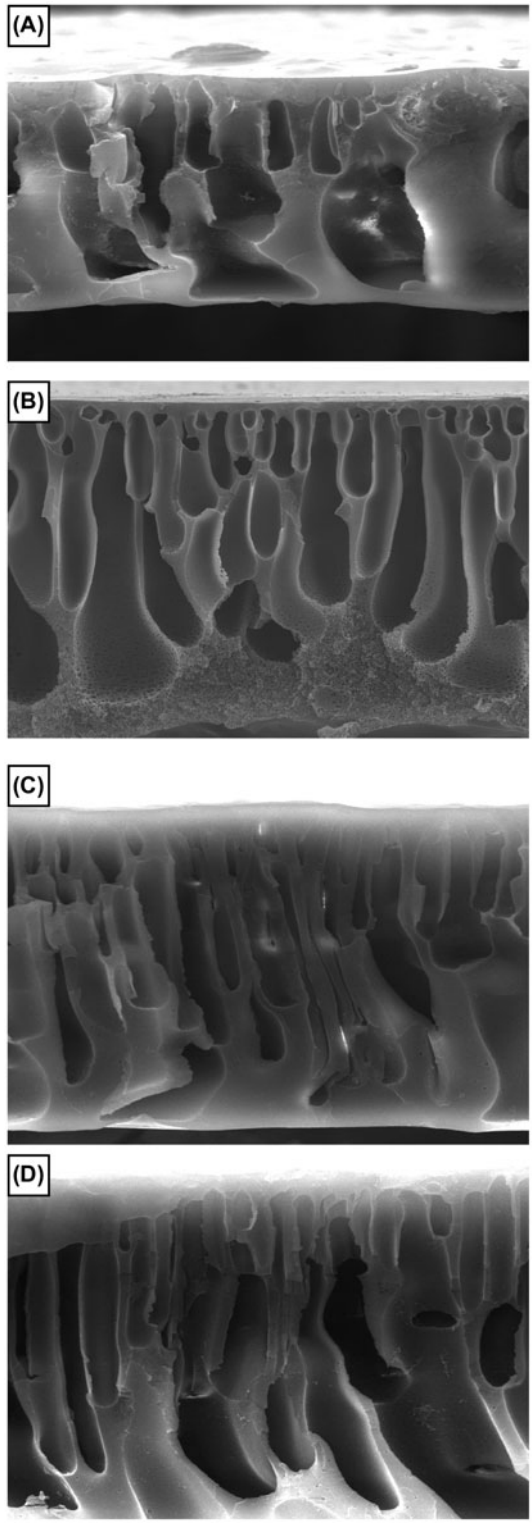


Fig. 4. The SEM images of 18 wt.% PAN membranes (cross section) at different coagulation bath temperatures: (A) 5℃, (B) 15℃, (C) 25℃, and (D) 35℃. The casting solution temperature was 50℃ and glass plate temperature was 20℃.

porosity of membrane prepared via the TIPS and CRINIPS were similar to that of membrane prepared via CRINIPS, and the BSA retention of the former was obviously higher than that of the latter. Fig. 7 shows the pore size distribution of membrane prepared via different membrane formation mechanisms. It can be concluded that the pore size of membrane prepared via combining TIPS and CRINIPS was more uniform than that of membrane prepared via CRINIPS, and the range of pore size distribution were 0.095–0.10 and 0.1–0.15 μm, respectively.

The existence of the above phenomenon can be attributed to the membrane morphology. By comparing Fig. 4(B), (D), and Fig. 6, it can be seen from that the structure (Fig. 4(B)) of membrane prepared via the combination of TIPS and CRINIPS was asymmetric possesses the advantages of high flux and BSA retention. That may be attributed to the effects of both heat transfer and chemical reaction introduced mass transfer when the hot casting solution was immersed into aqueous solution of 2 wt.% $NaHCO_3$ as coagulation bath media [29]. However, the pore morphology of membrane prepared via CRINIPS was straight-through (Fig. 4(D)). The reason may be bath temperature was higher and the faster heat transfer accelerated the chemical reaction during the gelation process. Fig. 4(A) shows the pore morphology of membrane prepared via the combination of TIPS and CRINIPS. While its structure was closed and unconnected which was different from Fig. 4(B). The reason may be that the cold coagulation bath promotes heat transfer. Then, the solid-liquid demixing appeared immediately which led to $CO_2$ generated from chemical reaction could not exude when the casting solution was immersed into coagulation bath (2% wt. $NaHCO_3$ (aq.)) [37]. Therefore, these phenomenon resulted in generation of closed and unconnected pore structure.

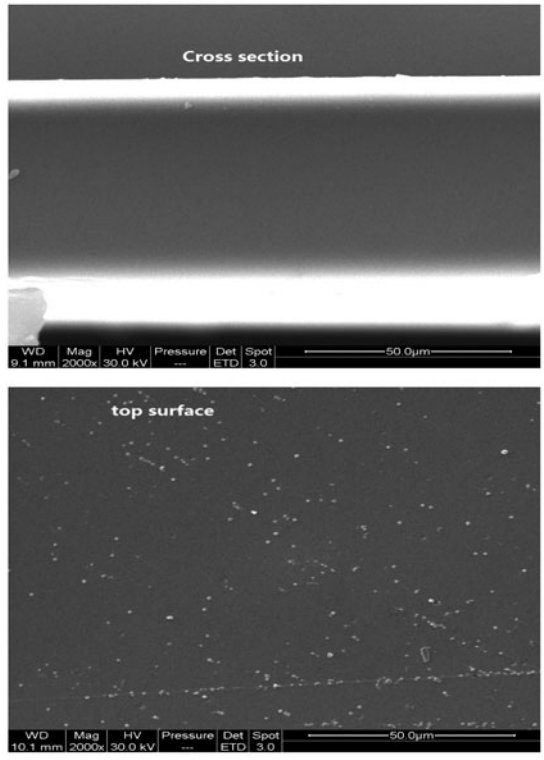


Fig. 6. The SEM images of 18 wt.% PAN membranes cooled from 50 to 15℃ via TIPS: cross section and top surface. The casting solution temperature was 50℃ and glass plate temperature was 20℃.

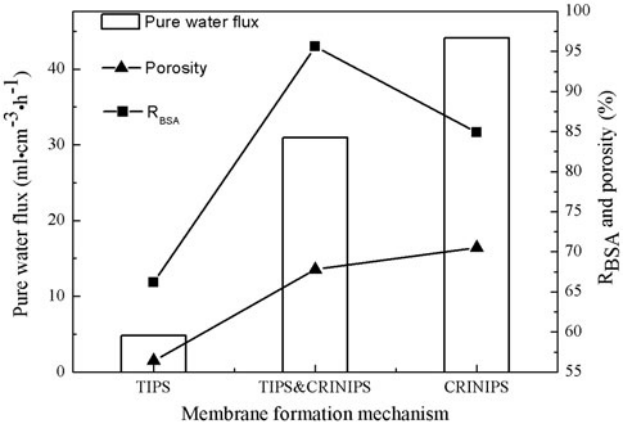


Fig. 5. Effect of membrane formation mechanism on pure water flux, BSA retention and porosity. The casting solution temperature was 5℃ and glass plate temperature was 20℃.

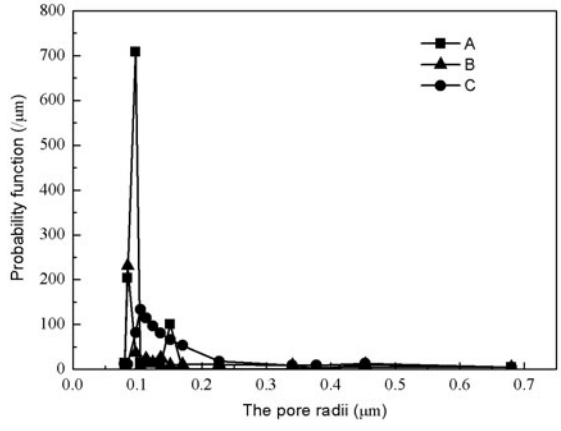


Fig. 7. The pore size distribution of membrane prepared via different membrane formation mechanism: (A) TIPS, (B) TIPS and CRINIPS, and (C) CRINIPS. The casting solution temperature was 50℃ and glass plate temperature was 20℃.

According to the above statement, the membrane performance could be enhanced dramatically by the combination of thermally- and chemical reaction introduced nonsolvent-induced phase separations. In the next section, the performance of membrane prepared via different membrane formation mechanisms will be analyzed using various fouling models.

### 3.3. The comparison of fouling mechanism for membrane prepared via different membrane formation mechanism

Membrane bioreactors (MBRs) have been successfully and extensively employed in municipal and industrial wastewater treatment owning to their low energy consumption, negligible phase change and so on [38,39]. However, the major operational problem is membrane biofouling, which limits their widespread application. So, it's essential to study the membrane fouling mechanism in order to understand membrane fouling performance fundamentally. Due to the complexity of extracted EPS in real MBR systems and lacking knowledge on the interactions between EPS and membrane materials, BSA was used as model protein because of its readily available in high purified form and the broadly investigations of its adsorption on a range of materials. The main objective of this part is to better understand fouling behavior of membranes prepared with different membrane formation mechanism mentioned in Section 3.2.

Most studies of protein fouling have interpreted the observed differences in flux decline during protein filtration using the classical pore blockage, pore constriction, and/or cake filtration models [40,41], and the models are illustrated in Table 3. In this part, the experiments were carried out under the transmembrane pressure of 0.1 MPa and filtration time of 60 min, the filtrate data of BSA through membranes prepared via different membrane formation mechanism were fitted to the four models by nonlinear regression method.

Table 3
The presentation of four models and their forms

| Number | Name | Fouling models | Description for constants and parameters |
|---|---|---|---|
| 1 | Complete pore blockage model | $\frac{J}{J_0} = \exp(-aJ_0AC_bt)$ | $a$ is parameter |
| 2 | Intermediate pore blockage model | $\frac{J}{J_0} = (1 + bJ_0AC_bt)^{-1}$ | $b$ is parameter |
| 3 | Pore constriction model | $\frac{J}{J_0} = (1 + cJ_0AC_bt)^{-2}$ | $c$ is parameter |
| 4 | Cake formation model | $\frac{J}{J_0} = (1 + dJ_0C_bt)^{-1/2}$ | $d$ is parameter |

Notes: $J_0$ is the initial filtrate flux through the clean membrane, $A$ is the membrane surface area, $C_b$ is the bulk concentration of BSA, and t is the filtrate time.

In order to estimate the goodness-of-fit, four different nonlinear error functions ($R^2$, SSE, RMSE, chi-Square) were examined, and the constants and parameters in the four models were acquired by minimizing the four error functions. The values of $R^2$, SSE, RMSE, and chi-Square for BSA flux are presented in Table 4. As shown in Table 4, Cake filtration model

Table 4
Nonlinear regression parameters for fit of BSA flux (initial concentration = 100 mg/l)

| Number | Model | Membrane formation mechanism | $R^2$ | RMSE | Chi-Square | SSE |
|---|---|---|---|---|---|---|
| 1 | Complete pore blockage model | TIPS | 0.953 | 0.128 | 3.000 | 0.561 |
| | | CRINIPS | 0.951 | 0.131 | 3.331 | 0.615 |
| | | TIPS and CRINIPS | 0.967 | 0.134 | 4.216 | 0.749 |
| 2 | Intermediate pore blockage model | TIPS | 0.968 | 0.068 | 0.590 | 0.159 |
| | | CRINIPS | 0.965 | 0.074 | 0.770 | 0.197 |
| | | TIPS and CRINIPS | 0.978 | 0.078 | 1.119 | 0.257 |
| 3 | Pore constriction model | TIPS | 0.959 | 0.113 | 1.665 | 0.350 |
| | | CRINIPS | 0.957 | 0.106 | 2.002 | 0.405 |
| | | TIPS and CRINIPS | 0.972 | 0.111 | 2.716 | 0.516 |
| 4 | Cake formation model | TIPS | 0.981 | 0.034 | 0.035 | 0.040 |
| | | CRINIPS | 0.979 | 0.034 | 0.049 | 0.043 |
| | | TIPS and CRINIPS | 0.988 | 0.026 | 0.073 | 0.029 |

is the most appropriate, which provides a good fit to BSA filtrate data with high value of $R^2$ and the low values of RMSE and chi-Square related to other three models. It is well known that the smaller value of SSE indicates the better curve fitting. It can also be seen from Fig. 8 that for three different kinds of membranes prepared via membrane formation mechanism, cake filtration model is validated as the most suitable with SSE value of 0.029, 0.043, and 0.040, which is lower than that of other three models. This behavior can be attributed to the physical deposition of large protein aggregates on the membrane surface [42]. Besides, the SSE value in cake filtration model for the membrane prepared via combination of TIPS and CRINIPS was the smallest in Fig. 8. The reason may be that the membrane pore structures prepared via combination of TIPS and CRINIPS was asymmetric and interconnected (as shown in Fig. 4(B)), while the pore structures of membranes prepared with TIPS and CRINIPS were straight-through (as shown in Figs. 4(D) and 6) [43] This conclusion was in accordance with the result which was mentioned in Section 3.2.

### 3.4. The effect of casting substrate temperature

In this part, the membranes of 18 wt.% PAN containing GA were prepared by varying the glass plate temperature, and the casting solution temperature was maintained at 50˚C. All the cast solutions were immersed into 15˚C aqueous solution of 2 wt.% $NaHCO_3$ as coagulation media to prepare the membranes via the combination of thermally- and chemical reaction introduced nonsolvent-induced phase separations (TIPS and CRINIPS). Fig. 9 illustrates pore morphology of the membranes which were prepared at different glass plate temperature (20, 50, and 80˚C). Fig. 10 presents the corresponding pore size distributions of the membranes by analyzing the pore sizes in the SEMs for each membrane. As shown in Fig. 10, the increasing of glass plate temperature resulted in bigger membrane pore size. When the glass plate temperature was 20˚C, the average pore size was approximately 0.097 μm (0.095–0.10 μm). When the temperature of glass plate increased to 50 and 80˚C, the average pore sizes were approximately 0.105 μm

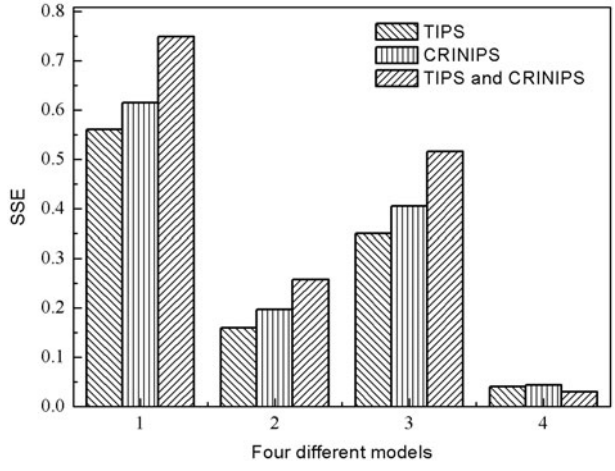


Fig. 8. The comparison of SSE of membrane prepared via different membrane formation mechanism for four different models.

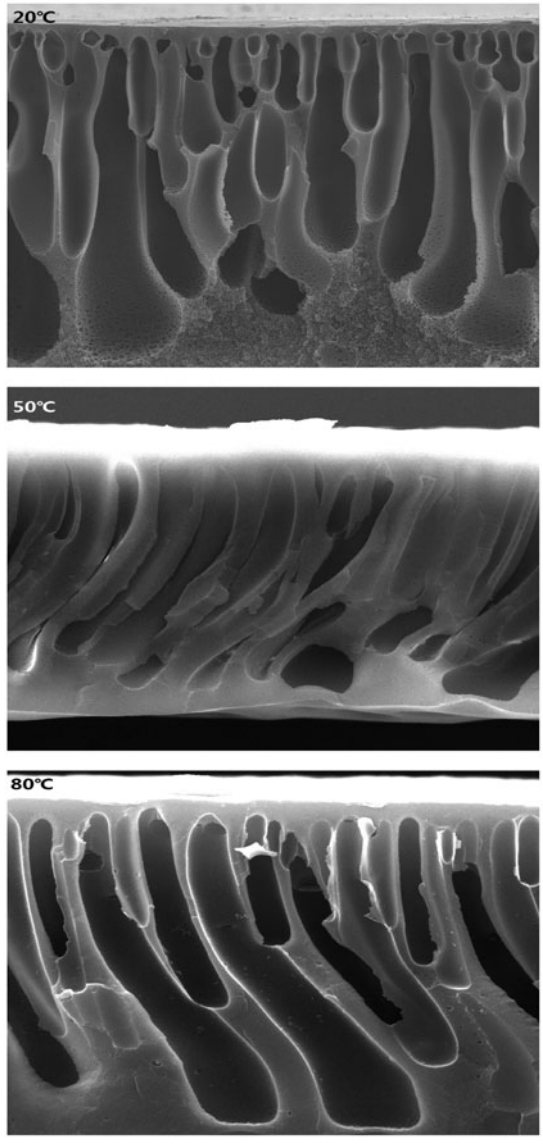


Fig. 9. The structure of membranes prepared by varying the glass plate temperature. The casting solution temperature was 50˚C.

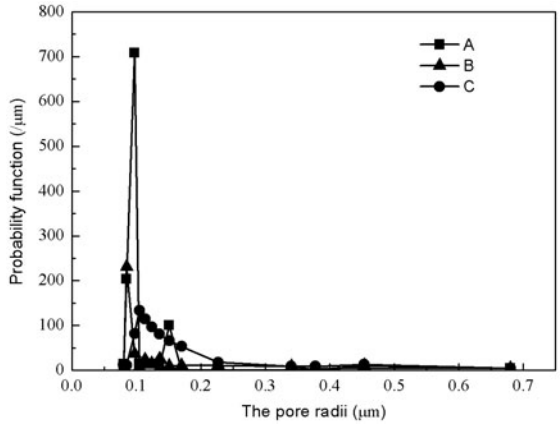


Fig. 10. The pore size distribution of membrane prepared by varying the glass plate temperature.

(0.1–0.11 μm) and 0.125 μm (0.11–0.136 μm), respectively. Fig. 11 presents the corresponding pure water flux and its BSA retention of the membranes. As shown in Fig. 11, pure water flux increased with the increasing of glass plate temperature. On the contrary, BSA retention decreased with increasing of glass plate temperature. These results were identified with the pore sizes shown in Fig. 9. When the glass plate temperature increased, the heat transfer between glass plate and casting solution was faster, meanwhile, the chemical reaction occurred. As a result, the faster heat transfer accelerated the chemical reaction, which resulted in the straight-through pore structures as shown in Fig. 9 (50 and 80˚C). When the glass plate temperature was lower, the heat transfer was slow. The membrane top-layer structure is thought to be formed via CRINIPS when the glass plate was

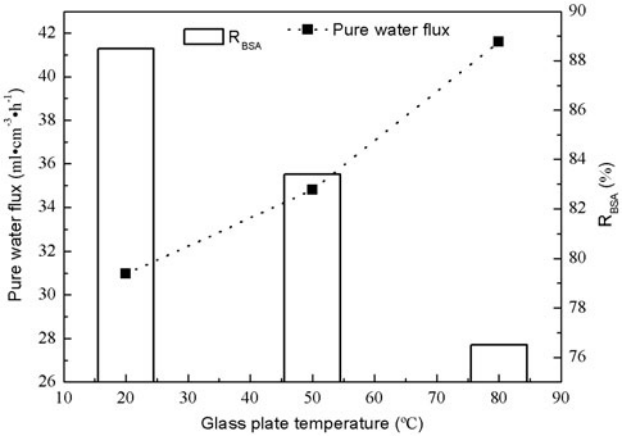


Fig. 11. Effect of glass plate temperature on pure water flux and BSA retention. The casting solution temperature was 50˚C.

immersed into the coagulation bath at 50˚C, because the casting solution was contacted with water which induces phase separation at 50˚C. On the other hand, the structure of the bottom is thought to be formed by TIPS because the glass plate on this side protected the casting solution against the water influx, while the polymer solution was cooled by the water bath (15˚C) thorough the glass plate [33].

## 4. Conclusions

Microporous PAN membranes with well-connected pore structure can be prepared via the combination of thermally and chemical reaction nonsolvent-induced phase separations (TIPS and CRINIPS). Coagulation bath temperature can significantly influence the membrane performance. When coagulation bath temperature was lowered from 35 to 15˚C, pore connectivity and asymmetry were significantly improved. When 15˚C aqueous solution of 2 wt.% $NaHCO_3$ as coagulation media was used and the temperature of casting solution and glass plate were 50 and 20˚C, respectively, a well-connected microporous membrane with high porosity could be obtained and its average pore size could be reduced to around 0.1 μm. However, membrane structure was closed and unconnected when coagulation bath temperature was lowered to 5˚C. The uniform PAN membrane which was exclusively formed via thermally induced phase separation (TIPS) had low porosity and both of the surface and cross-section were dense. Fouling model analysis showed that cake formation model is the most appropriate model for membranes prepared via different membrane formation mechanism, and SSE value in cake filtration model for the membrane prepared via TIPS and CRINIPS was the smallest which was related to asymmetric and interconnected membrane morphology. Glass plate temperature also played an important role in the formation of microporous PAN membranes. The pore structure was connective and asymmetric, and the average pore size reduced from about 0.125 to 0.097 μm when glass plate temperature decreased from 80 to 20˚C by using a 15˚C aqueous solution of 2 wt.% $NaHCO_3$ as coagulation bath media in membrane precipitation.

## Acknowledgment

Support for this work was provided by the Natural Science Foundation of Beijing (Project No. 2122009).

## Nomenclature

$J$ — the pure water flux (ml cm$^{-2}$ h$^{-1}$)
$V$ — the permeate volume of water (ml)
$S$ — the effective area of membrane (m$^2$)
$t$ — the time of obtaining the required volume (s)
$C_P$ — the concentration of the filtrate solution (g/l)
$C_F$ — the concentration of the feed solution (g/l)
$R$ — the membrane retention
$f(r)$ — the pore size distribution
$P_o$ — the porosity of the membrane (%)
$W_2$ — the weight of the wet membrane (g)
$W_1$ — the weight of the dry membrane (g)
$V$ — the volume of the membrane (cm$^3$)
$d_{water}$ — the water density at room temperature (g cm$^{-3}$)

*Greek symbols*

$\sigma$ — the surface tension of the n-butyl alcohol-water (N m$^{-1}$)
$\theta$ — the polymer-n-butyl alcohol contact angle (°)

## References

[1] S. Majeed, D. Fierro1, K. Buhr, J. Wind, B. Du, Multi-walled carbon nanotubes (MWCNTs) mixed polyacrylonitrile (PAN) ultrafiltration membranes, J. Membr. Sci. 403–404 (2012) 101–109.
[2] D. Wang, K. Li, W.K. Teo, Preparation and characterization of polyvinylidene fluoride (PVDF) hollow fiber membranes, J. Membr. Sci. 163(2) (1999) 211–220.
[3] P. Sukitpaneenit, T.S. Chung, Molecular elucidation of morphology and mechanical properties of PVDF hollow fiber membranes from aspects of phase inversion, crystallization and rheology, J. Membr. Sci. 340 (1–2) (2009) 192–205.
[4] S. Rajabzadeh, T. Maruyama, T. Sotani, H. Matsuyama, Preparation of PVDF hollow fiber membrane from a ternary polymer/solvent/nonsolvent system via thermally induced phase separation (TIPS) method, Sep. Purif. Technol. 63(2) (2008) 415–423.
[5] G.L. Ji, C.H. Du, B.K. Zhu, Y.Y. Xu, Preparation of porous PVDF membrane via thermally induced phase separation with diluent mixture of DBP and DEHP, J. Appl. Polym. Sci. 105(3) (2007) 1496–1502.
[6] X. Lu, X. Li, Preparation of polyvinylidene fluoride membrane via a thermally induced phase separation using a mixed diluent, J. Appl. Polym. Sci. 114(2) (2009) 1213–1219.
[7] C.A. Dickey, J.E. Mcdaniel, Method of producing spherical thermoplastic particles, 1975, US 3896196.
[8] P. Georlette, J. Leva, Composition comprising a vinylidene fluoride polymer and a blowing agent, 1984, U.S. 4425443.
[9] M. Grasselli, N. Betz, Making porous membranes by chemical etching of heavy-ion tracks in [beta]-PVDF films, Nuclear Instruments and Methods in Physics Research Section B: Beam Interactions with Materials and Atoms, 236(1–4) (2005) 501–507.
[10] M. Mulder, Basic Principles of Membrane Technology, Kluwer Academic, Dordrecht, 1996.
[11] S. Huang, G. Wu, S. Chen, Preparation of microporous poly(vinylidene fluoride) membranes via phase inversion in supercritical $CO_2$, J. Membr. Sci. 293(1–2) (2007) 100–110.
[12] J.H. Cao, B.K. Zhu, G.L. Ji, Y.Y. Xu, Preparation and characterization of PVDF-HFP microporous flat membranes by supercritical $CO_2$ induced phase separation, J. Membr. Sci. 266(1–2) (2005) 102–109.
[13] C. Feng, K.C. Khulbe, T. Matsuura, R. Gopal, S. Kaur, S. Ramakrishna, M. Khayet, Production of drinking water from saline water by air-gap membrane distillation using polyvinylidene fluoride nanofiber membrane, J. Membr. Sci. 311(1–2) (2008) 1–6.
[14] R. Gopal, S. Kaur, Z. Ma, C. Chan, S. Ramakrishna, T. Matsuura, Electrospun nanofibrous filtration membrane, J. Membr. Sci. 281(1–2) (2006) 581–586.
[15] R.E. Kesting, Synthetic Polymeric Membranes: A Structural Perspective, Wiley, New York, NY, 1985.
[16] S.S. Kim, D.R. Lloyd, Microporous membrane formation via thermally-induced phase separation. III. Effect of thermodynamic interactions on the structure of isotactic polypropylene membranes, J. Membr. Sci. 64 (1991) 13–29.
[17] D.R. Lloyd, S. Soo, K.E. Kinzer, Microporous membrane formation via thermally induced phase separation. II. Liquid–liquid phase separation, J. Membr. Sci. 64 (1991) 1–11.
[18] Q.Y. Wu, L.S. Wan, Z.K. Xu, Structure and performance of polyacrylonitrile membranes prepared via thermally induced phase separation, J. Membr. Sci. 409–410 (2012) 355–364.
[19] H. Matsuyama, K. Ohga, T. Maki, M. Teramoto, S. Nakatsuka, Porous cellulose acetate membrane prepared by thermally induced phase separation, J. Appl. Polym. Sci. 89 (2003) 3951–3955.
[20] Z. Yang, P. Li, L. Xie, Z. Wang, S. Wang, Preparation of iPP hollow-fiber microporous membranes via thermally induced phase separation with co-solvents of DBP and DOP, Desalination 192 (2006) 168–181.
[21] H. Matsuyama, T. Maki, M. Teramoto, K. Asano, Effect of polypropylene molecular weight on porous membrane formation by thermally induced phase separation, J. Membr. Sci. 204 (2002) 323–328.
[22] H. Matsuyama, H. Okafuji, T. Maki, M. Teramoto, N. Kubota, Preparation of polyethylene hollow fiber membrane via thermally induced phase separation, J. Membr. Sci. 223 (2003) 119–126.
[23] M. Shang, H. Matsuyama, M. Teramoto, D.R. Lloyd, N. Kubota, Preparation and membrane performance of poly(ethylene-co-vinyl alcohol) hollow fiber membrane via thermally induced phase separation, Polymer 44 (2003) 7441–7447.
[24] T. Ishigami, K. Nakatsuka, Y. Ohmukai, Solidification characteristics of polymer solution during polyvinylidene fluoride membrane preparation by nonsolvent-induced phase separation, J. Membr. Sci. 438 (2013) 77–82.
[25] M. Wang, L. Wu, C.J. Gao, The influence of phase inversion process modified by chemical reaction on membrane properties and morphology, J. Membr. Sci. 270 (2006) 154–161.
[26] S. Wang, Z. Wang, Y. Zhang, W. Wu, D. Liu, X. Zhang, Experimental study of the control of pore sizes

of porous membranes applying chemicals methods, Desalination 177 (2005) 7–13.
[27] Y. Liang, Z. Wang, X. Ye, W. Li, X. Xi, L. Yang, X. Wang, J. Zhang, Y. Liu, Z. Cai, Study on the control of pore sizes of membranes using chemical methods. Part III: The performance of carbonates and bicarbonates in the membrane-making process by the chemical reaction, Desalination 267 (2011) 42–48.
[28] C. Zhou, Z. Wang, Y. Liang, J. Yao, Study on the control of pore sizes of membranes using chemical methods. Part II: Optimization factors for preparation of membranes, Desalination 225 (2008) 123–138.
[29] H. Matsuyama, Y. Takida, T. Maki, Preparation of porous membrane by combined use of thermally induced phase separation and immersion precipitation, Polymer 43 (2002) 5243–5248.
[30] C. Yen, H. He, L.J. Lee, Synthesis and characterization of nanoporous polycaprolactone membranes via thermally- and nonsolvent-induced phase separations for biomedical device application, J. Membr. Sci. 343 (2009) 180–188.
[31] T. Tanaka, T. Nishimoto, K. Tsukamoto, Formation of depth filter microfiltration membranes of poly(l-lactic acid) via phase separation, J. Membr. Sci. 396 (2012) 101–109.
[32] G. Capannelli, F. Vigo, S. Munari, Ultrafiltration membranes: Characterization methods, J. Membr. Sci. 15(3) (1983) 289–313.
[33] T. Tanaka, D.R. Lloyd, Formation of poly(l-lactic acid) microfiltration membranes via thermally induced phase separation, J. Membr. Sci. 238 (2004) 65–73.
[34] Sh Basha, B. Jha, Estimation of isothermparameters for biosorption of Cd(II) and Pb(II) onto brown seaweed, Lobophora ariegata, J. Chem. Eng. Data 53 (2008) 449–455.
[35] W.S.W. Ho, K.K. Sirkar (Eds.), Membrane Handbook, Chapman & Hall, New York, 1992.
[36] P. van de Witte, p.j. Dijkstra, J.W.A. van den Berg, Phase separation processes in polymer solutions in relation to membrane formation, J. Membr. Sci. 117 (1996) 1–31.
[37] D.R. Lloyd, K.E. Kinzer, H.S. Tseng, Microporous membrane formation via thermally induced phase separation. I. Solid–liquid phase separation, J. Membr. Sci. 52 (1990) 239–261.
[38] A.E. Contreras, A. Kim, Q.L. Li, Combined fouling of nanofiltration membranes: Mechanisms and effect of organic matter, J. Membr. Sci. 327 (2009) 87–95.
[39] C. Fersi, L. Gzara, M. Dhahbi, Flux decline study for textile wastewater treatment by membrane processes, Desalination 244 (2009) 321–332.
[40] J. Hermia, Constant pressure blocking filtration laws: Application to power law non-Newtonian fluids, Trans. Inst. Chem. Eng. 60 (1982) 183–187.
[41] L. Zeman, A.L. Zydney, Microfiltration and ultrafiltration: Principles and Applications, Marcel Dekker, New York, 1996.
[42] S.T. Kelly, W.S. Opong, A.L. Zydney, The influence of protein aggregates on the fouling of microfiltration membranes during stirred cell filtration, J. Membr. Sci. 80 (1993) 175.
[43] C.C. Ho, A.L. Zydney, Effect of membrane morphology on the initial rate of protein fouling during microfiltration, J. Membr. Sci. 155 (1999) 261–275.